Interactions between Al atoms on Al(110) from first-principles calculations

Yogesh Tiwary and Kristen A. Fichthorn*
Department of Chemical Engineering and Department of Physics, The Pennsylvania State University, University Park, Pennsylvania 16802, USA

(Received 13 February 2007; revised manuscript received 24 April 2007; published 29 June 2007)

We quantified pair and trio interactions between Al adatoms on the Al(110) surface using first-principles, density-functional theory, total-energy calculations. We find that the pair interaction is the strongest for the nearest in-channel $[1\bar{1}0]$ neighbor and is attractive due to the formation of direct chemical bonds between the adatoms. Beyond the nearest neighbor, the pair interaction is repulsive and is mediated by elastic distortion of the substrate atoms. The pair interaction is negligible for adatom separations beyond ~8.00 Å. Interactions between atoms in a collinear trio chain along the in-channel $[1\bar{1}0]$ direction have both electronic and elastic characters. All other trio interactions are elastic in origin. The long-ranged trio interaction is significant and exhibits damped oscillations between attraction and repulsion. We find several trios that enhance cross-channel [001] attraction. This trio attraction facilitates the formation of two-dimensional islands in Al(110) homoepitaxy, which are not favored by repulsive cross-channel pair interactions. These observations demand a refined approach to study thin-film growth, in which many-body interactions are taken into account.

DOI: 10.1103/PhysRevB.75.235451 PACS number(s): 68.35.Md, 71.15.Nc, 05.70.Np, 81.10.Aj

I. INTRODUCTION

Over a past few decades, self-organization at the nanometer scale has attracted much attention due to its proposed applications in nanotechnology. At present, however, the capability to induce and guide self-assembly at gas-solid interfaces remains elusive for most applications.[1] Since growth often occurs away from equilibrium, a knowledge of the kinetic processes governing the formation of thin-film morphology is essential for describing growth and predicting the structures that form. From a thermodynamic standpoint, knowledge of the atomic-scale interactions that dictate various assembled structures is also crucial. The elucidation of these interactions for the growth of Al on Al(110) is the topic of the present study.

Al/Al(110) homoepitaxy is an example of a system that exhibits nanoscale self-assembly.[2,3] At temperatures between 330 and 500 K and for a deposition rate of ~1 monolayer/min (ML/min), "nanohuts" with smooth {111} and {100} facets emerge after about 10 ML have been deposited. Upon further deposition, these huts subsequently grow and self-organize, reaching average heights of 50 nm after 30 ML has been deposited. An understanding of the fundamental interplay between interactions and kinetics in this nonequilibrium system will yield insight into the mechanisms of self-assembly. To this end, Zhu *et al.*[3] used *ab initio* calculations based on density-functional theory (DFT) to find the diffusion barriers for some of the relevant kinetic processes. They incorporated these processes into (1+1)-dimensional kinetic Monte Carlo (KMC) simulations of growth along the $[1\bar{1}0]$ direction and were able to show that huts arise due to low-energy barriers for adatoms to ascend step edges and to climb up to the top of the faceted islands. To move toward a *three-dimensional* description of growth, in which we can understand and predict hut sizes and shapes, as well as their spatial organization, it is of interest to understand the atomic-scale interactions that are extant in this system and how these influence the rates of the surface processes that lead to assembly. Below, we discuss the results of a first-principles study employing DFT to achieve the first of these objectives: elucidation of the interactions between Al adatoms on Al(110).

II. METHODS

To quantify adatom interactions, we utilized first-principles, total-energy calculations based on DFT, as implemented in the Vienna *ab initio* simulation package (VASP).[4–6] These calculations are based on ultrasoft Vanderbilt-type pseudopotentials,[7] as supplied by Kresse and Hafner,[8] the generalized gradient approximation (GGA) by Perdew and Wang,[9] and Fermi-Dirac smearing[10] with a width of 0.2 eV. An energy cutoff of 9.50 Ry (129.2 eV) is used for the plane-wave basis set, which is enough for the desired accuracy. To sample the Brillouin zone, we used the Monkhorst-Pack scheme.[11] Using a converged $(13\times13\times13)$ k-point mesh, we obtained a value for the bulk lattice constant of 4.05 Å, which is the same as the experimental value.[12]

To represent the Al(110) surface, we constructed a supercell consisting of a multilayered atomic slab with a vacuum spacing above the (110) surface and replicated it periodically in the three orthonormal symmetry directions. For all the total-energy calculations, the vacuum spacing is at least equal to the slab thickness in order to avoid the interaction between slabs normal to the surface. We obtained the optimized geometries by relaxing the slabs (including adatoms) until the forces on all unconstrained atoms are smaller than 0.04 eV/Å. We used two slabs having 5×3 and 3×5 surface atoms along the $[1\bar{1}0]\times[001]$ directions, each with a thickness of ten atomic layers. Atoms in the bottom five layers are fixed to their bulk locations calculated by using the obtained lattice constant. To reduce the slab thickness necessary for the desired accuracy, atoms are adsorbed only on one side of the slab. For an aluminum surface and adatoms, the emergence of an artificial electric field perpendicular to

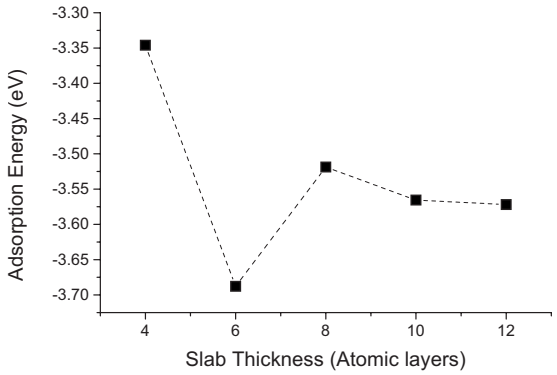

FIG. 1. Convergence of E_{ads} with increasing slab thickness.

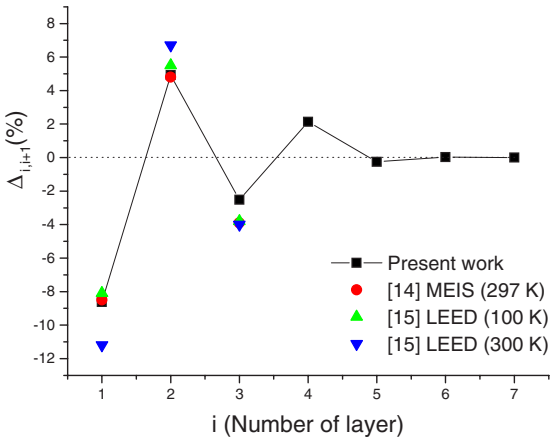

FIG. 2. (Color online) Oscillatory contraction-expansion for a 12-layer slab, in which the bottom six layers are constrained. $\Delta_{i,i+1}$ is the percentage change from the bulk interlayer spacing between the i and $i+1$ layers, where $i=1$ is the top layer.

the slab due to asymmetry is expected to be small, so that the total energy is practically unaffected.[13] We verified that this is true for the present case.

To show that a 10-layer slab is sufficient for the substrate and adatoms to relax fully, we calculated the adsorption energy E_{ads} of an Al atom using a 5×3 supercell by subtracting the total energy of a bare slab (substrate) E_s from the total energy of the substrate plus one adatom E_{s+1}, i.e.,

$$E_{ads} = E_{s+1} - E_s. \quad (1)$$

There is a negligible interaction between the adatom and its periodic images for this slab, as we will show below, so E_{ads} accurately represents the adsorption energy of an isolated adatom. We obtained E_{ads} for slabs with different thicknesses, in which atoms in the bottom half are constrained to their bulk positions and atoms in the top half plus the adatom are allowed to relax. A converged (see discussion below) $5\times6\times1$ k-point mesh was used for these calculations. In Fig. 1, we can see that the value of E_{ads} converges for a slab thickness of ten atomic layers. On increasing the slab thickness to 12 layers, the change in E_{ads} is just 0.17%.

We also obtained interlayer relaxations $\Delta_{i,i+1}$ for the slabs, where $\Delta_{i,i+1}$ is the percentage change from the bulk interlayer spacing between the i and $i+1$ layers and $i=1$ for the top layer. In Fig. 2, we show $\Delta_{i,i+1}$ as a function of layer i for a fully relaxed, bare 12-layer slab. A damped, oscillatory contraction-expansion occurs for the interlayer spacing. The value of Δ_{67} from our calculation is almost zero and the displacement from the bulk locations for layers 5 and 6 are 0.003 and 0.0005 Å, respectively. Thus, these layers are almost at the bulk positions, even after relaxation. For the 12-layer slab with an adatom on the top, the *maximum* displacements of atoms from the bulk positions in the fourth, fifth, and sixth layers are 0.074, 0.016, and 0.013 Å, respectively, while the *average* displacement of the sixth layer is less than 0.003 Å. These observations suggest that relaxing the top five layers of a 10-layer slab is sufficient to obtain the desired accuracy.

A damped, oscillatory interlayer spacing has also been reported experimentally[14–18] and in other theoretical studies.[19–25] Table I shows the values of Δ_{12}, Δ_{23}, and Δ_{34} from our calculations and selected experimental and theoretical results. The values of Δ_{12}, Δ_{23}, and Δ_{34} from our calculations match very closely with the experimental results obtained using medium-energy ion scattering (MEIS) (Ref. 14) and low-energy electron diffraction (LEED),[15] also shown in Fig. 2, and fare better than previous theoretical results. A major difference between our results and those from previous DFT studies appears to be our use of the GGA and ultrasoft pseudopotentials, in contrast to the GGA and full-potential linearized augmented plane-wave method in Ref. 19, and the local-density approximation (LDA) and norm-conserving pseudopotentials applied in the other works.[20–23] As ex-

TABLE I. Value of interlayer relaxation for Al(110) obtained in our work, as well as in experimental and previous theoretical studies. A negative value of $\Delta_{i,i+1}$ represents contraction.

Method	Temp. (K)	Δ_{12}	Δ_{23}	Δ_{34}
DFT (GGA)[a]	0	−8.61	+4.92	−2.52
DFT (GGA)[b]	0	−7.18	+3.87	−2.12
DFT (LDA)[c]	0	−10.0	+4.0	−3.0
DFT (LDA)[d]	0	−6.8	+3.5	−2.0
DFT (LDA)[e]	0	−5.35	+1.15	−3.04
eDFT (LDA)[f]	0	−7.4	+3.8	−2.5
EAM[g]	0	−10.47	+3.64	−2.93
EAM[h]	0	−10.4	+3.14	−2.75
Experimental MEIS[i]	297	−8.5	+4.8	−3.9
Experimental LEED[j]	100	−8.1	+5.5	−3.8
	300	−11.2	+6.7	−4.0

[a]This work.
[b]Reference 19.
[c]Reference 20.
[d]Reference 21.
[e]Reference 22.
[f]Reference 23.
[g]Reference 24.
[h]Reference 25.
[i]Reference 14.
[j]Reference 15.

TABLE II. k-point convergence test for 5×3 and 3×5 supercells.

5×3 supercell		3×5 supercell	
k points	E_{ads} (eV)	k points	E_{ads} (eV)
$3\times2\times1$	−3.590	$5\times2\times1$	−3.549
$5\times6\times1$	−3.566	$8\times3\times1$	−3.551
$6\times7\times1$	−3.566	$11\times5\times1$	−3.552

pected, our results exhibit better agreement with experiment than those based on the semiempirical embedded-atom method (EAM).[24,25]

We tested the convergence of the k-point mesh for both the 5×3 and 3×5 supercells by calculating the value of E_{ads} [cf., Eq. (1)] with increasing k-point density. The results of these tests are reported in Table II. Here, we can see that E_{ads} is absolutely converged for the k-point sampling of $5\times6\times1$ and $8\times3\times1$ for the 5×3 and 3×5 supercells, respectively. Differences in the value of E_{ads} for the two slabs are due to the interaction of the adatom with its periodic images for the 3×5 slab, as we will discuss below.

We quantified various pair and three-body (trio) interactions that can occur between adatoms on Al(110). Pair and trio interactions of interest are shown in Figs. 3 and 4, respectively. Pairs that are n sites apart along the in-channel $[1\bar{1}0]$ direction are denoted as I_n, while pairs that are m sites apart along the cross-channel [001] direction are denoted as C_m. The interaction energies associated with in- and cross-channel pairs are denoted as E_{I_n} and E_{C_m}, respectively. Diagonal pairs, for which adatoms are placed n sites apart in the in-channel and m sites apart in the cross-channel directions, are denoted as I_nC_m and their interaction energies are denoted as $E_{I_nC_m}$. The longest pair separation (d_{12}) considered is for pair I_3C_1, with a distance before relaxation of $d_{12}=9.49$ Å. As we will show below, the pair interaction becomes negligible for separations even shorter than this value.

Trios are characterized by the trio perimeter d_{123}, which is given by the sum of the three involved edges before relaxation, i.e., $d_{123}=d_{12}+d_{23}+d_{13}$, where d_{ij} is the separation between the ith and jth trio adatoms. The interaction energy for trio n (T_n) with perimeter $d_{123}(T_n)$ is denoted by E_{T_n} and trios are named in the order of increasing d_{123} [$d_{123}(T_1)<d_{123}(T_2)\cdots$]. The maximum value of d_{123} for the trios that we considered in this study is 20.55 Å (T_{14}). We considered all possible trios having d_{123} less than this value.

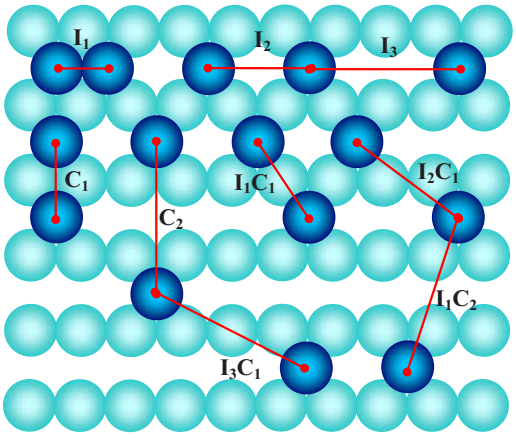

FIG. 3. (Color online) All the pair interactions quantified in this work.

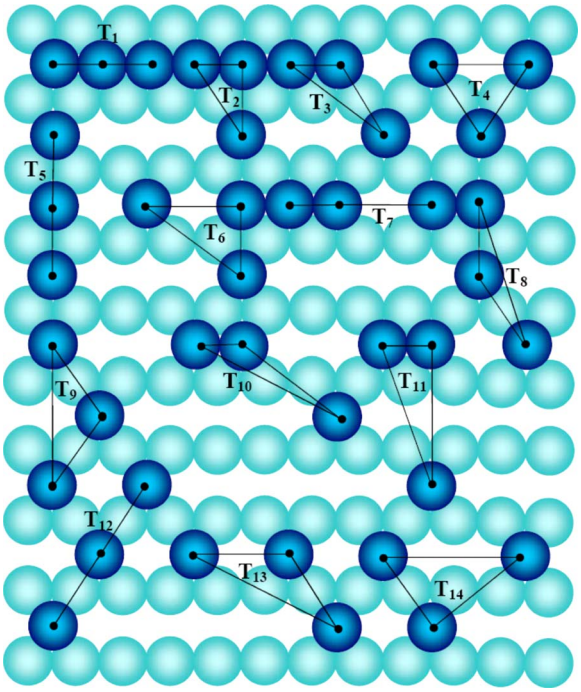

FIG. 4. (Color online) All the trio interactions quantified in this work.

To quantify the interaction energies between the desired pairs and trios, we constructed 23 distinct 5×3 and 3×5 supercells having different arrangements of adatoms over the substrate. All the desired pairs and trios are present at least once in either one of the main supercells or a combination of the main supercell and the periodic images. The 23 configurations are shown in Fig. 5, along with the one we used to obtain the adsorption energy [Fig. 5(a)]. The rectangular region in the upper left corner of each configuration in Fig. 5 shows the main supercell and the three other regions show all or part of the relevant periodic replicas. The total interaction energy ΔE between the adatoms is represented by a sum of all the pair E_{pair} and trio E_{trio} interactions between the adatoms in the main cell, as well as between atoms in the main cell and their periodic images, i.e.,

$$\Delta E = \sum E_{pair} + \sum E_{trio}. \quad (2)$$

Higher-order interactions (e.g., four body, five body, etc.) can also be significant on this surface[26,27] and we have tried to minimize their influence by limiting the adsorbate densities in the supercells shown in Fig. 5. Our initial analysis of four-body interactions[27] suggests that we do not have significant higher-order interactions in any of the supercells used for the present calculations. The total interaction energy is obtained in the DFT calculations using

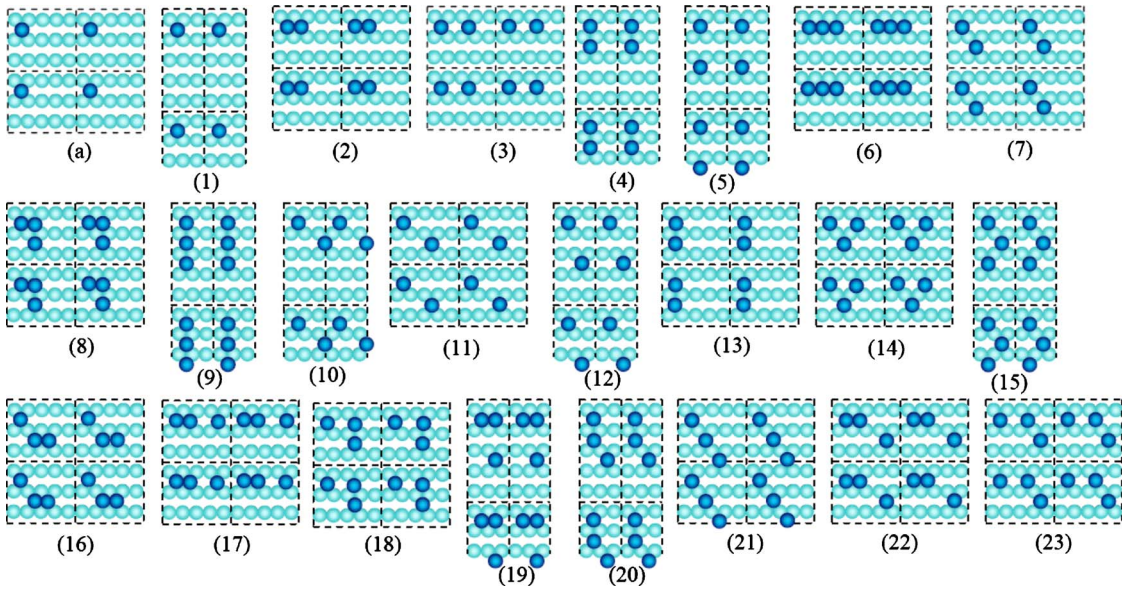

FIG. 5. (Color online) Supercell configurations used to formulate lattice-gas equations to quantify the pair and trio interactions of interest. The rectangular region at the top left corner of each configuration shows the main supercell and the three other regions show all or part of the relevant periodic replicas.

$$\Delta E = E_{s+n} - E_s - nE_{ads}, \tag{3}$$

where E_s is the energy of the bare slab, E_{s+n} is the energy of the substrate with n adatoms, and E_{ads} is the adsorption energy of a single adatom [cf., Eq. (1)]. Equating Eqs. (2) and (3) gives the lattice-gas equation

$$E_{s+n} - E_s - nE_{ads} = \Sigma E_{pair} + \Sigma E_{trio}. \tag{4}$$

For the sample configuration shown in Fig. 6, the lattice-gas equation can be constructed as

$$E_{s+3} - E_s - 3E_{ads} = (E_{I_1} + E_{C_1} + E_{I_1C_1} + E_{C_2} + E_{I_1C_2}) + (E_{T_2} + E_{T_{11}}). \tag{5}$$

Thus, we obtain 23 equations from the 23 unique supercell configurations. We find the values of the 23 interaction energies between 9 pairs and 14 trios by solving these equations.

Interactions between adatoms on surfaces can be either direct or indirect (substrate mediated) and the substrate-mediated interactions can have both electronic and elastic components.[28–42] In an attempt to distinguish the electronic and elastic contributions to the indirect interactions, we used an approach adopted in previous studies,[43–45] which employed two different relaxation schemes. In the first scheme, we place the adatoms on a prerelaxed and fixed substrate and then only the adatoms are allowed to optimize their positions. By fixing the substrate, we suppress its relaxation with respect to the adatoms and we eliminate the elastic contribution to the indirect interaction so we can quantify the electronic component. In the second scheme, we allow both the adatoms and the top five layers of the substrate to simultaneously relax to the optimized geometry. This yields the total interaction energy, consisting of both electronic and elastic components. The elastic component of the interaction can be estimated by subtracting the electronic component (from the first relaxation scheme) from the total interaction energy (from the second relaxation scheme). We note that these schemes do not perfectly delineate electronic and elastic interactions because the two may be coupled. Also, this distinction does not adequately quantify short-ranged, direct interactions associated with chemical bonds. Nevertheless, it does provide a means to estimate these two different effects.

III. RESULTS

The values obtained for the total, electronic, and elastic interaction energies for the pairs and trios shown in Figs. 3 and 4 are summarized in Table III. To confirm the convergence of the lattice-gas model, we compared its predictions for two additional supercells with new adatom configurations (shown in Fig. 7) to values obtained in additional *ab initio* calculations. The results of this comparison are shown in Table IV, where we see that interaction energies from the lattice-gas model match closely with the *ab initio* results. The maximum discrepancy between the two is 0.003 eV. This validates the lattice-gas model and indicates that our results are accurate.

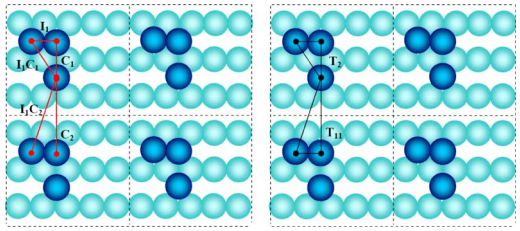

FIG. 6. (Color online) Interaction energies involved in supercell 8 shown in Fig. 5, for which a sample lattice-gas equation is shown in Eq. (5).

TABLE III. Values of the total, electronic, and elastic components of interaction energies of the pairs and trios shown in Figs. 3 and 4. A negative value of the interaction energy denotes attraction.

		Interaction energy (eV)		
Pair/trio	d_{12}/d_{123}	Total	Electronic	Elastic
I_1	2.86	−0.104	−0.237	0.133
C_1	4.05	0.038	−0.008	0.046
I_1C_1	4.96	0.033	0.008	0.026
I_2	5.72	0.029	0.003	0.026
I_2C_1	7.01	0.036	−0.001	0.037
C_2	8.09	−0.002	−0.002	0.000
I_1C_2	8.58	−0.005	−0.004	−0.001
I_3	8.59	0.015	−0.002	0.017
I_3C_1	9.49	−0.004	0.003	−0.007
T_1	11.45	−0.006	0.054	−0.060
T_2	11.87	−0.060	−0.006	−0.054
T_3	14.83	−0.044	−0.003	−0.041
T_4	15.64	−0.021	−0.002	−0.019
T_5	16.19	0.032	0.007	0.025
T_6	16.78	−0.019	−0.001	−0.018
T_7	17.17	−0.025	−0.004	−0.020
T_8	17.59	0.011	0.002	0.008
T_9	18.00	0.019	0.002	0.017
T_{10}	19.36	−0.005	0.000	−0.006
T_{11}	19.54	0.015	0.003	0.012
T_{12}	19.83	0.004	0.002	0.003
T_{13}	20.17	0.017	0.000	0.017
T_{14}	20.55	−0.017	0.000	−0.017

Figure 8 shows the pair interaction as a function of separation d_{12}. Here, we see that the magnitude of the pair interaction decreases with increasing separation. Beyond the nearest, in-channel neighbor (I_1), which has attraction, the pair interaction is repulsive or negligible. The strong, short-range attraction for I_1 results from the formation of direct, chemical bonds between the two neighboring adatoms. This can be seen in a plot of the charge density associated with I_1,

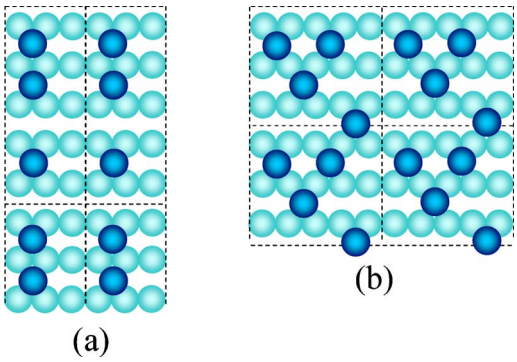

FIG. 7. (Color online) Additional configurations used to validate the lattice gas model.

TABLE IV. Comparison between interaction energies from *ab initio* calculations and the lattice-gas model for the additional supercells shown in Fig. 7.

	Ab initio		*Lattice-gas model*	
Configuration	Total	Electronic	Total	Electronic
a	0.073	−0.012	0.070	−0.012
b	0.172	0.017	0.175	0.016

shown in Fig. 9. Atoms relevant for our discussion are numbered in the top-down view in Fig. 9(a). Evidence for a direct, electronic interaction can be seen for I_1 from the charge buildup between adatoms 1 and 2 in Fig. 9(b). These two adatoms are closer than the bulk spacing by 0.07 Å, and they reside further above the surface than an isolated adatom. In comparing the charge density of an isolated adatom [shown in Fig. 10(b)] with the adatom pair I_1 [Fig. 9(b)], the charge distribution between the adatom and the substrate atoms is different for the pair (and the difference is more prominent toward the center of the pair) than that for an isolated adatom. These observations support the rebonding theory.[46,47] We observed a relatively weaker charge buildup between adatoms in the pair C_1, explaining a much smaller value of the electronic component of this interaction energy (−0.008 eV), and we did not observe charge buildup for the pair I_2, marking the end of the direct, electronic interaction.

With the exception of I_1, the electronic component of the pair interaction is negligible and the long-range contribution to the total interaction energy is dominated by the elastic component due to the perturbation of the substrate atoms around the adatoms. These results contrast those for the Ag(111) and Cu(111) surfaces, which possess Shockley surface states that can be characterized as a nearly free electron gas. Through first-principles calculations based on DFT, Fichthorn and Scheffler[43] and Luo and Fichthorn[44] determined that the interaction is primarily electronic in origin for Ag(111). Bogicevic *et al.*,[45] Stepanyuk *et al.*,[48] as well as Stasevich *et al.*[49] came to similar conclusions for pair interactions on Cu(111). In DFT studies of the pair interaction on Al(111) and Cu(001), which do not possess a Shockley sur-

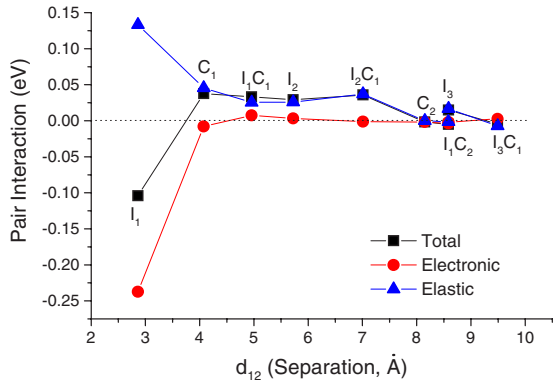

FIG. 8. (Color online) Pair interaction as a function of separation, d_{12}.

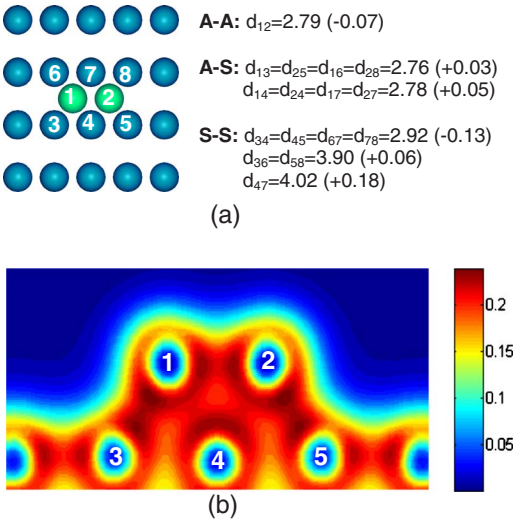

FIG. 9. (Color online) Atom relaxation and charge distribution for the pair I_1. In (a), the top-down view indicates relevant (numbered) atoms in the pair interaction. The separations (in Å) between adatom-adatom (A-A), adatom-substrate atom (A-S), and substrate atom-substrate atom (S-S) pairs are reported for selected pairs. Quantities in brackets indicate the difference (in Å) from the bulk value for A-A and difference from an isolated adatom for A-S and S-S. In (b), the charge density (in $e/\text{Å}^3$) is shown in a plane that cuts approximately through the centers of atoms 1–5.

face state, the conclusion was still that the pair interaction is primarily electronic in origin.[45,49]

To further investigate the range of pairwise elastic interactions, an adatom is adsorbed over a (larger) slab having ten layers with 8×5 atoms per layer. This large slab is used to completely eliminate the interaction of the adatom with its periodic images. The perturbations of the surface atoms normal to and along the surface plane after being relaxed using

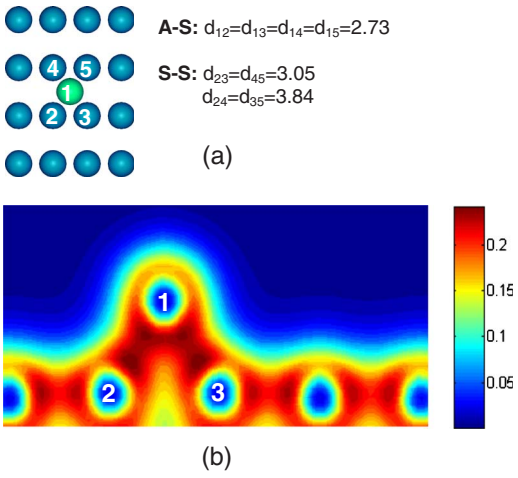

FIG. 10. (Color online) Atom relaxation and charge distribution for an isolated adatom. In (a), the top-down view indicates relevant (numbered) atoms for an isolated adatom. The separations (in Å) between adatom-substrate atom (A-S) and substrate atom-substrate atom (S-S) pairs are reported for selected pairs. In (b), the charge density (in $e/\text{Å}^3$) is shown in a plane that cuts approximately through the centers of atoms 1–3.

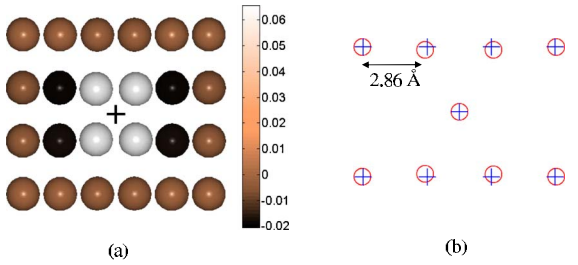

FIG. 11. (Color online) Relaxations of surface atoms induced by the presence of an adatom: (a) Displacements normal to the surface plane: the cross in the center shows the position of the adatom and the heights (in Å) of the surrounding surface atoms relative to those of the bare surface are indicated on the scale. (b) Displacements in the surface plane: the positions of the atoms in a bare substrate are indicated by circles and the relaxed positions in the presence of an adatom are indicated by crosses.

a $2\times2\times1$ k-point mesh are shown in Fig. 11. In Fig. 11(a), we can see that the four base atoms in contact with the adatom move up (+0.06 Å) and the in-channel neighbors of these four atoms move down (−0.02 Å) relative to atoms in the bare surface. The four base atoms in direct contact with the adatom are also the most displaced from their initial positions in the surface plane compared to the other surface atoms, as seen from Fig. 11(b). Thus, an adatom creates a perturbation zone extending up to its second in-channel and first cross-channel neighbor site. This perturbation can induce a substrate stress and change the adsorption energy of another adatom in this zone, leading to an effective adsorbate-adsorbate interaction. The maximum range of elastic interactions can be approximated as two times the size of this zone: i.e., if the perturbation zones of two adatoms do not overlap, then they behave like isolated adatoms. This limit is reached for I_4 in the in-channel direction (11.45 Å) and C_2 in the cross-channel direction (8.09 Å). From Fig. 8, we can see that the pair interaction becomes negligible for separations greater than ~8.0 Å, supporting the analysis.

Investigating the classical elastic distortion of an isotropic substrate using a continuum model, Lau and Kohn[33] predicted that the long-range, elastic interaction between two identical adatoms is always repulsive and decays with the separation d_{12} as d_{12}^{-3}. Although we find that the elastic pair interaction is repulsive (or negligible) here, we do not observe the d_{12}^{-3} decay predicted by Lau and Kohn. We note that Stoneham,[50] Lau and Kohn,[34] and Kappus[51] showed that for an anisotropic surface, the elastic interaction between identical adatoms can also be attractive if the anisotropic forces due to one adatom dilate the regions compressed by the other one. Attractive elastic interactions have been found in a number of previous studies.[34,52–55] Recent studies employing discrete-lattice dynamics predict a nonmonotonic decay of the elastic pair interaction with separation, even along a fixed crystallographic direction.[52,53,56–58] Our results provide another example of a deviation of the elastic pair interaction from the d_{12}^{-3} decay predicted by the original work of Lau and Kohn.[33]

A final important point regarding the pair interaction is that there is a strong attraction between the nearest in-

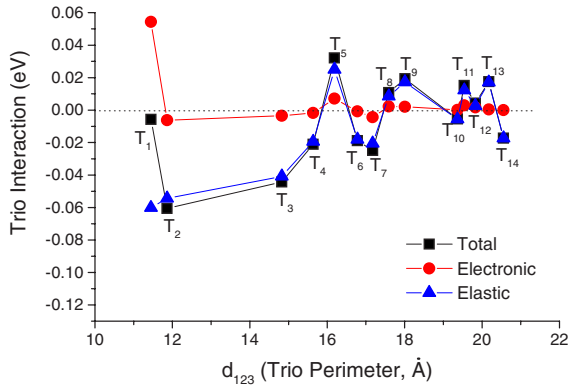

FIG. 12. (Color online) Trio interaction as a function of trio perimeter, d_{123}.

channel neighbors, but all the cross-channel and diagonal interactions are repulsive or negligible. Thus, these *pair* interactions do not support the formation of nanohuts observed experimentally in Al(110) homoepitaxy,[2,3] as adatoms have no attraction to help them stick and form islands with a significant extent in the cross-channel direction. This anomaly can be explained by the presence of many-body interactions.

Figure 12 shows the trio interaction as a function of the trio perimeter d_{123}. The trio interaction has an oscillatory decay with increasing d_{123}. With the exception of E_{T_1}, the trios have negligible electronic components and are elastic in origin. We see that the trio interaction is small at the longest separations studied, but it is still not negligible. To ensure a negligible trio interaction, the three trio atoms should be separated by distances greater than those dictated by the perturbation zone shown in Fig. 11. Although such distances are too long to be considered in our study, we note that several of the trios are negligible at shorter separations.

Our finding of an elastic trio interaction contrasts results from DFT studies of the (111) surfaces of Ag and Cu, where trios were found to be primarily electronic in origin.[44,49] The total interaction energy of the collinear trio T_1 is mildly attractive in spite of having the maximum independent contributions of the electronic and elastic interactions. This matches qualitatively with the DFT results for collinear trios on the Cu(100) and Cu(111) surfaces[49] which were found to be attractive, being of moderate to small magnitudes.

The oscillations in the elastic interaction between attraction and repulsion might be due to the net surface stress induced by the trios. If the net effect relaxes the stress, then trios can have a negative interaction energy. Recently, Longo *et al.*[55] found that the stress induced by Fe clusters on Cu(111) substrates matches with the oscillations in the interaction energy. The mesoscopic mismatch between islands and substrate leading to a strong inhomogeneous stress and strain distribution has also been proposed for homoepitaxy on Cu(111).[59,60] The net perturbation of substrate atoms can also change the direct interactions between the adatoms. Thus, trio interaction can be attributed to a combination of these effects. Interestingly, we see that the repulsive cross-channel and diagonal interactions that we found for pairs are mitigated by attractive trios containing these bonds (e.g., T_2, T_3, T_4, T_6, and T_{14}). This indicates that trio interactions can play a crucial role in the nucleation of two-dimensional islands in Al/Al(110) homoepitaxy.

For various systems, previous experimental work using field-ion microscopy (FIM) and calculations based on semiempirical EAM potentials revealed a transition from linear chains to islands as the cluster size increases.[61–66] Experimentally (with FIM), the structure of Pt clusters on Pt(100) was observed to oscillate between chain and island configurations as the number of Pt adatoms increased from 3 to 6.[63] In EAM studies of Pt and Pd clusters on Pt(100),[63,64] this transition was attributed to four-body interactions. Stable Ir and Re trimers were also experimentally observed on W(110) with FIM,[61,62,65] in spite of repulsive pairs. In this system, the chain-island transition of the Ir clusters was interpreted in terms of three-body interactions. In recent EAM studies, which probed the chain to island transition on several different fcc(110) surfaces using the genetic algorithm, this transition was interpreted in terms of pair interactions. Our work shows that three-body (and possibly higher-order[27]) interactions can play a crucial role in this transition for Al/Al(110). KMC simulations of growth almost always consider only pair interactions and it is apparent that pair models are not satisfactory for the growth of such systems.

IV. CONCLUSIONS

We quantified pair and trio interactions between Al adatoms on the Al(110) surface using DFT total-energy calculations. We find that the pair interaction is the strongest for the nearest in-channel $[1\bar{1}0]$ neighbor and is attractive, primarily due to a direct electronic interaction. Beyond the nearest neighbor, the pair interaction is elastic in origin and it is repulsive. The pair interaction becomes negligible for adatom separations beyond ~8.00 Å. With the exception of the collinear trio chain along the in-channel $[1\bar{1}0]$ direction, the trio interaction is elastic in origin. The long-ranged trio interaction is significant and exhibits damped oscillations between attraction and repulsion. Interestingly, several key attractive trios are associated with the formation of cross-channel [001] bonds. This trio attraction is apparently important for the formation of two-dimensional structures in Al(110) homoepitaxy, as the cross-channel pair interaction is repulsive. These observations demand a refined approach to study thin-film epitaxial growth, in which many-body contributions are taken into account when simulating adatom diffusion. Future work along this line can help us gain more insight into the atomic-scale mechanisms of self-assembly.

ACKNOWLEDGMENTS

This work has been supported by the National Science Foundation Grant No. DMR 0514336. This work was partially supported by the National Center for Supercomputing Applications under Grant No. TG-DMR060049N and utilized the NCSA's IBM pSeries 690 cluster.

*Email address: fichthorn@psu.edu

[1] K. A. Fichthorn and M. Scheffler, Nature (London) **429**, 617 (2004).
[2] F. Buatier de Mongeot, W. Zhu, A. Molle, R. Buzio, C. Boragno, U. Valbusa, E. G. Wang, and Z. Y. Zhang, Phys. Rev. Lett. **91**, 016102 (2003).
[3] W. Zhu, F. B. de Mongeot, U. Valbusa, E. G. Wang, and Z. Y. Zhang, Phys. Rev. Lett. **92**, 106102 (2004).
[4] G. Kresse and J. Hafner, Phys. Rev. B **47**, 558 (1993).
[5] G. Kresse and J. Furthmüller, Comput. Mater. Sci. **6**, 15 (1996).
[6] G. Kresse and J. Furthmüller, Phys. Rev. B **54**, 11169 (1996).
[7] D. Vanderbilt, Phys. Rev. B **41**, 7892 (1990).
[8] G. Kresse and J. Hafner, J. Phys.: Condens. Matter **6**, 8245 (1994).
[9] J. P. Perdew and Y. Wang, Phys. Rev. B **45**, 13244 (1992).
[10] N. D. Mermin, Phys. Rev. **137**, A1441 (1965).
[11] H. J. Monkhorst and J. D. Pack, Phys. Rev. B **13**, 5188 (1976).
[12] *AIP Handbook*, 3rd ed., edited by D. E. Gray (McGraw-Hill, New York, 1987).
[13] R. Stumpf and M. Scheffler, Phys. Rev. B **53**, 4958 (1996).
[14] B. W. Busch and T. Gustafsson, Surf. Sci. **415**, L1074 (1998).
[15] A. Mikkelsen, J. Jiruse, and D. L. Adams, Phys. Rev. B **60**, 7796 (1999).
[16] J. N. Andersen, H. B. Nielsen, L. Petersen, and D. L. Adams, J. Phys. C **17**, 173 (1984).
[17] J. R. Noonan and H. L. Davis, Phys. Rev. B **29**, 4349 (1984).
[18] H. Göbel and P. von Blanckenhagen, Phys. Rev. B **47**, 2378 (1993).
[19] J. L. F. Da Silva, Phys. Rev. B **71**, 195416 (2005).
[20] R. N. Barnett, U. Landman, and C. L. Cleveland, Phys. Rev. B **28**, 1685 (1983).
[21] K. M. Ho and K. P. Bohnen, Phys. Rev. B **32**, 3446 (1985).
[22] A. G. Eguiluz, Phys. Rev. B **35**, 5473 (1987).
[23] N. Marzari, D. Vanderbilt, A. De Vita, and M. C. Payne, Phys. Rev. Lett. **82**, 3296 (1999).
[24] T. Ning, Q. Yu, and Y. Ye, Surf. Sci. **206**, L857 (1988).
[25] S. P. Chen, D. J. Srolovitz, and A. F. Voter, J. Mater. Res. **4**, 62 (1989).
[26] T. L. Einstein, R. Sathiyanarayanan, and T. J. Stasevich, http://meetings.aps.org/link/BAPS.2007.MAR.H42.10
[27] Y. Tiwary and K. A. Fichthorn (unpublished).
[28] J. Koutecky, Trans. Faraday Soc. **54**, 1038 (1958).
[29] T. B. Grimley, J. Am. Chem. Soc. **90**, 3016 (1968).
[30] T. B. Grimley, Proc. Phys. Soc. London **90**, 751 (1967).
[31] T. B. Grimley, Proc. Phys. Soc. London **92**, 776 (1967).
[32] T. L. Einstein and J. R. Schrieffer, Phys. Rev. B **7**, 3629 (1973).
[33] K. H. Lau and W. Kohn, Surf. Sci. **65**, 607 (1977).
[34] K. H. Lau and W. Kohn, Surf. Sci. **75**, 69 (1978).
[35] T. L. Einstein, in *Chemistry and Physics of Solid Surfaces II*, edited by R. Vaneslow (CRC, Boca Raton, FL, 1979), p. 261.
[36] T. L. Einstein, Surf. Sci. **84**, L497 (1979).
[37] T. L. Einstein, in *Handbook of Surface Science*, edited by W. N. Unertl (Elsevier, Amsterdam, 1996), Vol. 1, p. 577.
[38] T. L. Einstein, Surf. Sci. **75**, L161 (1978).
[39] P. Hyldgaard and M. Persson, J. Phys.: Condens. Matter **12**, 2981 (2000).
[40] P. Hyldgaard and T. L. Einstein, Europhys. Lett. **59**, 265 (2002).
[41] P. Hyldgaard and T. L. Einstein, Surf. Sci. **532-535**, 600 (2003).
[42] M. L. Merrick, W. Luo, and K. A. Fichthorn, Prog. Surf. Sci. **72**, 117 (2003).
[43] K. A. Fichthorn and M. Scheffler, Phys. Rev. Lett. **84**, 5371 (2000).
[44] W. Luo and K. A. Fichthorn, Phys. Rev. B **72**, 115433 (2005).
[45] A. Bogicevic, S. Ovesson, P. Hyldgaard, B. I. Lundqvist, H. Brune, and D. R. Jennison, Phys. Rev. Lett. **85**, 1910 (2000).
[46] P. J. Feibelman, Phys. Rev. Lett. **58**, 2766 (1987).
[47] A. Bogicevic, Phys. Rev. Lett. **82**, 5301 (1999).
[48] V. S. Stepanyuk, A. N. Baranov, D. V. Tsivlin, W. Hergert, P. Bruno, N. Knorr, M. A. Schneider, and K. Kern, Phys. Rev. B **68**, 205410 (2003).
[49] T. J. Stasevich, T. L. Einstein, and S. Stolbov, Phys. Rev. B **73**, 115426 (2006).
[50] A. M. Stoneham, Solid State Commun. **24**, 425 (1977).
[51] W. Kappus, J. Phys. C **11**, L565 (1978).
[52] S. C. Tiersten, T. L. Reinecke, and S. C. Ying, Phys. Rev. B **39**, 12575 (1989).
[53] S. C. Tiersten, T. L. Reinecke, and S. C. Ying, Phys. Rev. B **43**, 12045 (1991).
[54] L. E. Shilkrot and D. J. Srolovitz, J. Mech. Phys. Solids **45**, 1861 (1997).
[55] R. C. Longo, V. S. Stepanyuk, and J. Kirschner, J. Phys.: Condens. Matter **18**, 9143 (2006).
[56] R. Brako and D. Šokčevič, Surf. Sci. **469**, 185 (2000).
[57] R. Brako and D. Šokčevič, Surf. Sci. **454-456**, 623 (2000).
[58] R. Brako and D. Šokčevič, Vacuum **61**, 89 (2001).
[59] O. V. Lysenko, V. S. Stepanyuk, W. Hergert, and J. Kirschner, Phys. Rev. Lett. **89**, 126102 (2002).
[60] O. V. Lysenko, V. S. Stepanyuk, W. Hergert, and J. Kirschner, Phys. Rev. B **68**, 033409 (2003).
[61] H.-W. Fink and G. Ehrlich, J. Chem. Phys. **81**, 4657 (1984).
[62] F. Watanabe and G. Ehrlich, J. Chem. Phys. **96**, 3191 (1992).
[63] P. R. Schwoebel, S. M. Foiles, C. L. Bisson, and G. L. Kellogg, Phys. Rev. B **40**, 10639 (1989).
[64] A. F. Wright, M. S. Daw, and C. Y. Fong, Phys. Rev. B **42**, 9409 (1990).
[65] S. J. Koh and G. Ehrlich, Surf. Sci. **423**, L207 (1999).
[66] Z. Sun, Q. Liu, Y. Li, and J. Zhuang, Phys. Rev. B **72**, 115405 (2005).